HHS Public Access

Author manuscript

Acad Radiol. Author manuscript; available in PMC 2017 March 18.

Published in final edited form as:

Acad Radiol. 2012 December ; 19(12): 1554–1565. doi:10.1016/j.acra.2012.07.006.

Reproducibility of Four-dimensional Computed Tomography-based Lung Ventilation Imaging

Tokihiro Yamamoto, PhD, **Sven Kabus, PhD**, **Jens von Berg, PhD**, **Cristian Lorenz, PhD**, **Melody P. Chung, BS**, **Julian C. Hong, MS**, **Billy W. Loo Jr., MD, PhD**, and **Paul J. Keall, PhD**

Department of Radiation Oncology, Stanford University School of Medicine, 875 Blake Wilbur Dr., Stanford, CA 94305-5847 (T.Y., M.P.C., J.C.H., B.W.L.); Department of Digital Imaging, Philips Research Europe, Hamburg, Germany (S.K., J.v.B., C.L.); Sydney Medical School, University of Sydney, Sydney, NSW, Australia (P.J.K.)

Abstract

Rationale and Objectives—A novel ventilation imaging method based on four-dimensional (4D) computed tomography (CT) has been applied to the field of radiation oncology. Understanding its reproducibility is a prerequisite for clinical applications. The purpose of this study was to quantify the reproducibility of 4D CT ventilation imaging over different days and the same session.

Materials and Methods—Two ventilation images were created from repeat 4D CT scans acquired over the average time frames of 15 days for 6 lung cancer patients and 5 minutes for another 6 patients. The reproducibility was quantified using the voxel-based Spearman rank correlation coefficients for all lung voxels and Dice similarity coefficients (DSC) for the spatial overlap of segmented high-, moderate-, and low-functional lung volumes. Furthermore, the relationship between the variation in abdominal motion range as a measure of the depth of breathing and variation in ventilation was evaluated using linear regression.

Results—The voxel-based correlation between the two ventilation images was moderate on average (0.50 ± 0.15). The DSCs were also moderate for the high- (0.60 ± 0.08), moderate- (0.46 ± 0.06), and low-functional lung (0.58 ± 0.09). No patients demonstrated strong correlations. The relationship between the motion range variation and ventilation variation was found to be moderate and significant.

Conclusions—We investigated the reproducibility of 4D CT ventilation imaging over the time frames of 15 days and 5 minutes and found that it was only moderately reproducible. Respiratory variation during 4D CT scans was found to deteriorate the reproducibility. Improvement of 4D CT imaging is necessary to increase the reproducibility of 4D CT ventilation imaging.

Keywords

Deformable image registration; four-dimensional (4D) CT; functional imaging; lung; reproducibility; ventilation

Address correspondence to: P.J.K.: Paul.Keall@sydney.edu.au; and B.W.L.: BWLoo@stanford.edu.

In recent years, there have been significant advances in molecular and functional imaging as applied to the field of radiation oncology. The most important applications include treatment planning, especially for dose painting (ie, boosting dose to active tumor subregions) (1–3) and functional avoidance (ie, sparing dose from high-functional subregions of normal tissues) (4–6). The other important application is the assessment of tumor response to treatment (7) and radiation-induced normal tissue injury (8–10). In lung cancer radiotherapy, lung ventilation or perfusion imaging with single photon emission computed tomography (SPECT) (4, 11–19) and magnetic resonance (MR) (5,20–23) have been used in such applications. However, SPECT and MR imaging suffer from drawbacks such as low resolution, high cost, long scan time, and limited availability.

Lung ventilation images can be created by a novel technique based on four-dimensional (4D) computed tomography (CT) (24). The 4D CT-derived ventilation can be considered “free” information for lung cancer radiotherapy patients, because 4D CT scans are currently in routine use for treatment planning purposes at many centers (42.3%) (25) and ventilation computation involves only image processing and analysis. Moreover, 4D CT ventilation imaging has higher resolution, lower cost, shorter scan time, and/or higher availability compared to SPECTor MR imaging. In the literature, there have been several applications of 4D CT ventilation imaging to functional avoidance (6,26) and assessment of radiation-induced ventilation changes (27,28). Four-dimensional CT ventilation images have been found to vary widely with deformable image registration (DIR) algorithms and ventilation metrics (29), indicating the need for careful validation. Nevertheless, little validation has been performed to date. Several investigators evaluated the physiologic accuracy of 4D CT ventilation imaging by comparing with xenon CT ventilation imaging for animal subjects and found reasonable correlations (30–32). Major drawbacks of these studies include limited axial coverage (~3 cm). Castillo et al (33) and Yamamoto et al (34) compared 4D CT and SPECT ventilation images for thoracic cancer patients. Although they observed some regional agreements, the correlations were low overall, which was at least in part due to central airway depositions of the SPECT radiotracer (ie, technetium-99m-labeled diethylenetriamine pentaacetate) aerosols. Positive data on human subjects include significantly lower 4D CT ventilation in emphysematous regions (ie, known low-signal regions) than in nonemphysematous regions (ie, known high-signal regions) for 12 lung cancer patients as demonstrated by Yamamoto et al (35). More recently, Castillo et al compared 4D CT ventilation and SPECT perfusion images for 10 lung cancer patients and demonstrated strong correlations in functional defect regions distal to airway obstruction because of gross tumor (36). These results indicate the potential for a high physiologic accuracy of 4D CT ventilation imaging. Given the lack of data showing strong correlations with ground truth ventilation imaging for human subjects, however, further studies are necessary. In addition, the reproducibility should also be investigated, which is particularly important for longitudinal studies such as the assessment of radiation-induced ventilation changes. Recently, Du et al investigated the reproducibility of 4D CT ventilation imaging using repeat 4D CT scans acquired over less than 10 minutes for three anesthetized, mechanically ventilated sheep and nine lung cancer patients (37). They found high reproducibility for sheep, but relatively poor reproducibility for patients.

The purpose of this study was to assess the reproducibility of 4D CT ventilation imaging using repeat 4D CT scans acquired over two different time frames: different days (different-day cohort) and same session (same-session cohort). First, we investigated the hypothesis: 4D CT ventilation is constant with time in the absence of therapeutic intervention. Second, we performed a further analysis to investigate the hypothesis: the temporal variation in 4D CT ventilation is related to the temporal variation in abdominal motion range to identify an important factor that influences the reproducibility.

Material and Methods

Patients

We studied 12 patients who were enrolled on two different prospective clinical studies (six patients for each study) approved by the Institutional Review Board. All patients provided written informed consent. The primary objective of one of the two study protocols was to develop physiologically accurate 4D CT ventilation imaging; that of the other protocol was to investigate the role of a novel respiratory training system based on audiovisual biofeedback on 4D imaging. The two protocols essentially had equivalent inclusion and exclusion criteria, in which most patients with lung cancer of any histology to be treated by radiotherapy would be eligible. Patients underwent two repeat 4D CT scans before radiotherapy treatment on different days for the first protocol (different-day cohort), or immediately in the same session for the second protocol (same-session cohort). The rationale for the different-day scans was to model potential variations from image acquisition and underlying physiologic change.

4D CT Ventilation Imaging

Four-dimensional CT ventilation imaging consists of the following three steps: 1) acquisition of a 4D CT image set, 2) DIR for spatial mapping of the peak-exhale CT image to the peak-inhale image, and 3) quantification of regional volume change, yielding a ventilation image projected onto the peak-exhale phase. Each patient underwent two repeat 4D CT scans; therefore, two 4D CT ventilation images corresponding to the two time points were created per patient. Each of the three steps is described in detail here.

The first step was the acquisition of a 4D CT image set for 10 respiratory phase-based bins. Four-dimensional CT images are created by 1) acquiring oversampled CT data segments consisting of multiple slices simultaneously with an external respiratory signal and 2) retrospectively reconstructing a number of three-dimensional CT image sets correlated with a given respiratory displacement range or phase range. In our department, 4D CT scans are in routine use for thoracic and abdominal cancer. We acquired 4D CT scans of the entire thorax on a Discovery ST multislice positron emission tomography/CT scanner (GE Healthcare, Waukesha, WI) in cine mode. Simultaneously, a real-time position management (RPM) system (Varian Medical Systems, Palo Alto, CA) was used to measure patient's abdominal displacements by monitoring an infrared reflective box throughout a scan. Scan parameters were set as follows: 120 kVp, approximately 100 mAs per slice, 0.5-second gantry rotation, 0.45-second cine interval, and 2.5-mm slice thickness, as used clinically in our radiation oncology department. The CT data were continuously acquired for a cine

duration that was approximately 1 second longer than the estimated patient's respiratory period. Because the axial coverage of the scanner was 2 cm, the cine CT acquisition was performed at multiple couch positions such that the entire thorax was covered. GE Advantage 4D software was used to create a 4D CT image set by sorting CT slices based on the RPM phase information into 10 respiratory bins, yielding 10 three-dimensional CT volumes. In this study, we used paired CT images at the peak-exhale and peak-inhale phases for ventilation computation. Further details on the 4D CT image acquisition have been described elsewhere (38).

The second step was DIR for spatial mapping of the peak-exhale CT image to the peak-inhale image, deriving a displacement vector field (DVF). In this study, we used a volumetric elastic registration method that minimizes both a similarity function (sum of squared difference between the peak-inhale and deformed peak-exhale CT images) and a regularizing term (elastic regularizer) based on the Navier-Lame equation (39). The registration accuracy was previously investigated through quantifying the target registration error (distances between the anatomic landmarks [ie, vessel and bronchial bifurcations]) at the target phase propagated manually from the reference phase and those propagated by DIR. The target registration errors were found to be less than the voxel dimension on average (39–41). The same algorithm parameters used in these studies were employed in the current study as well.

The final step was the quantification of regional volume change through analyzing a DVF. In this study, we investigated the Jacobian-based ventilation metric (29,31–33,35). The Jacobian determinant (J) of the displacement vector, u, is given by

$$J(x,y,z)=\begin{vmatrix} 1+\frac{\partial u_x(x,y,z)}{\partial x} & \frac{\partial u_x(x,y,z)}{\partial y} & \frac{\partial u_x(x,y,z)}{\partial z} \\ \frac{\partial u_y(x,y,z)}{\partial x} & 1+\frac{\partial u_y(x,y,z)}{\partial y} & \frac{\partial u_y(x,y,z)}{\partial z} \\ \frac{\partial u_z(x,y,z)}{\partial x} & \frac{\partial u_z(x,y,z)}{\partial y} & 1+\frac{\partial u_z(x,y,z)}{\partial z} \end{vmatrix}, \quad (1)$$

which represents the differential contraction or expansion at point (x, y, z). The volume of each exhale voxel deformed into the inhale phase $\mathrm{Vol}_{\mathrm{in}}^{\mathrm{voxel}}$ can be estimated by

$$\mathrm{Vol}_{\mathrm{in}}^{\mathrm{voxel}}(x,y,z)=\mathrm{Vol}_{\mathrm{ex}}^{\mathrm{voxel}}(x,y,z)\cdot J(x,y,z), \quad (2)$$

where $\mathrm{Vol}_{\mathrm{ex}}^{\mathrm{voxel}}$ is the exhale voxel volume. In this study, the ventilation metric (V) was defined as exhale-to-inhale volume change and can be expressed as

$$V(x,y,z)=\mathrm{Vol}_{\mathrm{in}}^{\mathrm{voxel}}(x,y,z)-\mathrm{Vol}_{\mathrm{ex}}^{\mathrm{voxel}}(x,y,z)=\mathrm{Vol}_{\mathrm{ex}}^{\mathrm{voxel}}\cdot\{J(x,y,z)-1\}. \quad (3)$$

A value of zero corresponds to local volume preservation. A negative value represents local contraction, and a positive value represents local expansion. Thus 4D CT ventilation images at the peak-exhale phase were created for the first (V_{1st}) and second (V_{2nd}) scans. Further details on each step of 4D CT ventilation imaging have been described elsewhere (29,35).

The ventilation values outside the segmented lung parenchyma volumes have been zeroed before quantifying the reproducibility. The lung volume was segmented by delineating lung voxels, of which the HU values were smaller than a threshold of −250 in a similar manner to Guerrero et al (42) and Castillo et al (36) within the lung outlines generated by the model-based segmentation of the Pinnacle^3 treatment planning system (Philips Radiation Oncology Systems, Fitchburg, WI). Manual trimming of the central airways and great vessels was also performed where necessary.

Quantification of the Tidal Volume

The tidal volume was calculated from the 4D CT images to investigate variation in repeat 4D CT scans. First, the air volumes in the peak-exhale and peak-inhale lungs were estimated by integrating the air volumes of all the lung voxels for each phase. The air volume ($\mathrm{Vol}^{\mathrm{air}}$) in the voxel at location (*x, y, z*) is estimated by

$$\mathrm{Vol}^{\mathrm{air}}(x,y,z) = -\frac{\mathrm{HU}\,(x,y,z)}{1000}\mathrm{Vol}^{\mathrm{voxel}}(x,y,z), \quad (4)$$

where HU is the Hounsfield unit value (43). Note that the air and tissue densities were assumed to be −1000 and 0 HU, respectively. Second, the air volume in the peak-exhale lung was subtracted from that of the peak-inhale lung to determine a tidal volume.

Quantification of the Reproducibility of 4D CT Ventilation Imaging

The first and second 4D CT ventilation images were compared to assess the reproducibility. For longitudinal imaging studies, images acquired at different time points must be registered to a common reference domain before quantitative analysis. In this study, the same DIR method described above was used to propagate the peak-exhale CT image of the second scan to that of the first scan. The resulting DVF was then directly used to propagate the second ventilation image to the domain of the first image, given that the original 4D CT and ventilation images have exactly the same dimension and resolution. The reproducibility of 4D CT ventilation imaging was assessed qualitatively by visually comparing the two ventilation images and quantitatively using two metrics:

1. Voxel-based Spearman rank correlation coefficients (p) for all voxels within the lung
2. Dice similarity coefficients (DSC) (44) for the spatial overlap of segmented functional (high, moderate, and low) lung volumes as defined by

$$\mathrm{DSC}=\frac{2\cdot \mathrm{FLV}_{1\mathrm{st}}\cap \mathrm{FLV}_{2\mathrm{nd}}}{\mathrm{FLV}_{1\mathrm{st}}+\mathrm{FLV}_{2\mathrm{nd}}}, \quad (5)$$

where *FLV* is the segmented high-, moderate-, or low-functional lung volume.

For comparing two ventilation images acquired at different time points, normalization is necessary because of the temporal change in patient's breathing level. The ventilation values as determined by Equation 3 were globally normalized by the overall mean ventilation ($\bar{V}$) at each time point as:

$$V(x,y,z)=\frac{\mathrm{Vol}_{\mathrm{ex}}^{\mathrm{voxel}}\{J(x,y,z)-1\}}{\overline{V}}. \quad (6)$$

The high-, moderate-, and low-functional lung volumes were segmented by 1) computing a cumulative distribution function of the ventilation values within the lung; 2) calculating the ranges of ventilation values for the high, moderate, and low function such that the number of voxels for each was equivalent; and 3) delineating lung voxels, of which the ventilation values fall into each range using the Pinnacle^3 system. The cutoff values described in the literature have been employed to interpret the Spearman correlation coefficients and DSCs. Zou et al proposed the following cutoff values for the Spearman correlation coefficient: $\rho = 1.0$ as perfect, $0.8 \le \rho < 1.0$ as strong, $0.5 \le \rho < 0.8$ as moderate, $0.2 \le \rho < 0.5$ as weak, and $0 \le \rho < 0.2$ as no correlation (45). For the DSC, we used the following cutoff values: $0.8 < \mathrm{DSC} \le 1.0$ as almost perfect, $0.6 < \mathrm{DSC} \le 0.8$ as substantial, $0.4 < \mathrm{DSC} \le 0.6$ as moderate, $0.2 < \mathrm{DSC} \le 0.4$ as fair, $0 \le \mathrm{DSC} \le 0.2$ as slight, and $\mathrm{DSC} < 0$ as poor overlap, which are identical to the cutoff values for the kappa statistic proposed by Landis and Koch (46), considering that DSC is a special case of the kappa statistic (47).

Regression Analysis for the Relationship between the Abdominal Motion Range Variation and 4D CT Ventilation Variation

Given that the 4D CT–derived ventilation depends on the depth of breathing (Eq 3), a further analysis was performed to test the hypothesis: temporal variation in 4D CT ventilation is related to the temporal variation in abdominal motion range during 4D CT scans in order to identify an important factor that influences the reproducibility. The temporal variation in 4D CT ventilation (ΔV) was determined for each peak-exhale voxel by subtracting the first ventilation from the second ventilation as expressed by

$$\Delta V\,(x,y,z)=V_{2\mathrm{nd}}\,(x,y,z)-V_{1\mathrm{st}}\,(x,y,z)\,. \quad (7)$$

The temporal variation in abdominal motion range (Δm) was also determined for each peak-exhale voxel. The abdominal motion range was used as a measure of the depth of breathing and was determined based on abdominal displacements. Each CT data segment is assigned a

particular RPM-measured abdominal displacement at the moment of scan. The motion range was determined by calculating the difference between the peak-exhale and peak-inhale abdominal displacements. A link between the peak-exhale and peakinhale voxels was established using the same DVF calculated in ventilation imaging. The variation in motion range (Δm) was determined in a similar manner to the variation in ventilation by subtracting the first motion range (m) globally normalized by the overall mean ($\bar{m}$) from the second motion range normalized by the overall mean as expressed by

$$\Delta m(x,y,z)=\frac{m_{2\mathrm{nd}}(x,y,z)}{\overline{m_{2\mathrm{nd}}}}-\frac{m_{1\mathrm{st}}(x,y,z)}{\overline{m_{1\mathrm{st}}}}. \quad (8)$$

Note that the second ventilation or motion range images were propagated to the domain of the first scan in a similar manner to quantify the reproducibility when calculating temporal variations in ventilation or motion range.

Linear regression analysis was then performed to evaluate the global and regional relationship between the abdominal motion range variation and 4D CT ventilation variation. For the global relationship, the standard deviation of motion range variations (Δm) for all voxels within the lung was quantified as a global measure of the variation in the depth of breathing. The voxel-based correlation coefficients between the first and second 4D CT ventilation images were used as a global measure of the ventilation variation. For the regional relationship, the ventilation variations (ΔV) were averaged over the region with a particular motion range variation, considering that the abdominal displacement was a global measure for each CT data segment. The motion range variations were binned into intervals of 0.1 (eg, −0.15 to −0.05, −0.05 to +0.05, +0.05 to +0.15), ranging from the 5th percentile to the 95th percentile. The average ventilation variation was then determined for each bin of motion range variation. The cutoff values proposed by Zou et al have been employed to interpret the coefficient of determination (r^2): $r^2 = 1.0$ as perfect, $0.64 \le r^2 < 1.0$ as strong, $0.25 \le r^2 < 0.64$ as moderate, $0.04 \le r^2 < 0.25$ as weak, and $0 \le r^2 < 0.04$ as no correlation (45). Furthermore, we also investigated the impact of abdominal motion range–based linear normalization of the 4D CT ventilation on the reproducibility. The ventilation value was linearly normalized by the corresponding motion range value for each voxel as expressed by

$$V_m(x,y,z)=\frac{V(x,y,z)}{m(x,y,z)}. \quad (9)$$

Results

Patients

Basic characteristics of 12 patients and repeat 4D CT scans are described in Table 1. For the different-day cohort, the first scans were acquired as part of routine treatment simulation in a treatment position for all patients. The second scans were acquired on different days over the

average time frame of 15 days. The second scans were acquired before the start of lung cancer radiotherapy treatment for all patients, except for patients 4 and 6 who received the scans after delivering 7% (3.7 Gy) and 5% (3 Gy) of the prescribed dose, respectively, because of scheduling reasons. Radiation-induced changes in regional ventilation would be minimal considering low-dose levels. To accommodate another objective of the study protocol, the patients were asked to bring their arms down and the immobilization devices were not used in the second scans for patients 1, 2, 3, and 6. For the same-session cohort, the two scans were acquired in the same session without changing the patient position over the average time frame of 5 minutes. The use of audiovisual biofeedback was switched from the first scan to the second scan.

There were significant differences in the air volumes between the two scans at both the peak-exhale (first 3498 ± 1659 cm^3 vs. second 264 ± 1251 cm^3, $P < .01$) peak-inhale phases (3957 ± 1646 cm^3 vs. 3465 ± 1288 cm^3, $P < .01$). However, the lung volumes were comparable at both the peak-exhale (4384 ± 1804 cm^3 vs. 4321 ± 1862 cm^3, $P = .62$) and peak-inhale phases (4872 ± 1793 cm^3 vs. 4920 ± 1919 cm^3, $P = .67$). The tidal volumes (ie, the difference between the peak-exhale and peakinhale air volumes) were also comparable (460 ±144 cm^3 vs. 501 ± 171 cm^3, $P = .17$). The abdominal motion ranges as measured by the RPM system were comparable as well (0.79 ± 0.23 cm vs. 0.81 ± 0.31 cm, $P = .85$).

Reproducibility of 4D CT Ventilation Imaging

Figure 1 shows a comparison of the first and second 4D CT ventilation images for patient 1 of the same-session cohort, which demonstrated a moderate voxel-based Spearman correlation coefficient of 0.75 that was the highest in that cohort. In general, there were visually good agreements in the distributions of high (right lower and left upper lobes) and low ventilation (right upper and middle lobes) between the two images. However, considerable disagreements were also observed in several regions, especially around the left lower lobes. The DSCs for the segmented functional lung volumes were substantial or moderate (0.72, 0.59, and 0.76 for the high-, moderate-, and low-functional lung, respectively). Another comparison of the first and second 4D CT ventilation images for patient 6 of the different-day cohort is shown in Figure 2, which demonstrated a weak voxel-based correlation of 0.36 that was the lowest in that cohort. Although there were some agreements between the two ventilation images, the disagreements were more apparent throughout the lungs in contrast to patient 1 of the same-session cohort. For example, the right lower lobe clearly changed from a homogeneous distribution of high ventilation in the first scan to an inhomogeneous distribution in the second scan. The DSCs for the segmented functional lung volumes were moderate (0.54, 0.44, and 0.53 for the high-, moderate-, and low-functional lung, respectively). Table 2 shows a summary of the voxelbased Spearman correlation coefficients and DSCs for the 12 patients. On average, the voxel-based correlation was found to be moderate (0.50 ± 0.15), and the DSCs were also moderate (0.60 ± 0.08, 0.46 ± 0.06, and 0.58 ± 0.09 for the high-, moderate-, and low-functional lung, respectively). The correlations for the different-day cohort were comparable to those for the same-session cohort (voxel-based correlation, 0.48 ± 0.11 vs. 0.53 ± 0.20, $P = .50$). None ofthe 12 patients demonstrated either a strong voxel-based correlation or DSC between the

two ventilation images. The moderate-functional lung volumes demonstrated lower DSCs compared to the high- and low-functional lung volumes consistently in all patients.

Relationship between the Abdominal Motion Range Variation and 4D CT Ventilation Variation

Figure 3 shows a comparison ofthe abdominal motion range images of the first scan, second scan, and variation between the two scans for the same patients as those in Figures 1 and 2. Patient 1 of the same-session cohort demonstrated motion ranges close to 1 (ie, overall mean throughout the lungs), whereas patient 6 of the different-day cohort showed motion ranges considerably deviated from 1 in both the first and second scans. As a result, the motion range variation image of patient 1 of the same-session cohort demonstrated smaller variations with the standard deviation of 0.21 compared to 0.41 of patient 6 of the different-day cohort. Figure 4 shows the relationship between the standard deviation of motion range variation as a global measure of the variation in the depth of breathing and voxel-based Spearman correlation coefficients between the two 4D CT ventilation images for the 12 patients, indicating a moderate, statistically significant linear relationship ($r^2 = 0.55$, $P < .01$).

Figure 5a shows a comparison of the images of abdominal motion range variation and 4D CT ventilation variation for patient 2 of the different-day cohort. Visually, there were good correlations between the two images especially in the upper lobes, where the ventilation variation increased with increasing motion range variation. From linear regression analysis, the relationship between the motion range variation and ventilation variation was found to be strong and statistically significant for this particular case ($r^2 = 0.90$, $P < .01$; Fig 5b). Another comparison for patient 6 of the differentday cohort is shown in Figure 6, which demonstrated no relationship ($r^2 = 0.01$, $P = .83$). Even though there were visually remarkable disagreements throughout the lungs, there were some agreements around the upper lobes. Table 3 shows a summary of the linear regression analysis results for the 12 patients. The relationship between the motion range variation and ventilation variation was found to be statistically significant and strong for 4 patients, moderate for 2 patients, and weak for 1 patient. Five patients showed nonsignificant relationships. Overall, a moderate, significant relationship was observed based on all patients ($r^2 = 0.42$, $P < .01$).

Figure 7 shows a comparison of the first and second 4D CT ventilation images with and without abdominal motion range–based linear normalization. This particular case demonstrated a slight improvement in the correlation between the two ventilation images from 0.50 (voxel-based) without normalization to 0.56 with normalization. However, overall, motion range–based linear normalization resulted in the mean voxel-based correlation coefficient of 0.48 ± 0.20, which was comparable to 0.50 ± 0.15 without normalization ($P = .15$).

Discussion

An investigation on the reproducibility of 4D CT ventilation imaging over two different time frames, 15 days (differentday) and 5 minutes (same-session), was performed using repeat 4D CT scans for 12 lung cancer patients. Overall, the correlations between the repeat 4D CT

ventilation images were found to be moderate based on the voxel- and segment-wise analyses. Also, the correlations for the different-day cohort were comparable to those for the same-session cohort. None of the 12 patients demonstrated strong correlations between the repeat ventilation images. Recently, Du et al quantified the reproducibility of 4D CT ventilation imaging over the time frame of less than 10 minutes for three anesthetized, mechanically ventilated sheep and 9 lung cancer patients (37). They found high reproducibility for sheep, but relatively poor reproducibility for patients, which is consistent with our results. There have been several studies quantifying the reproducibility of other ventilation imaging modalities, including hyperpolarized ^{3}He MR imaging (48–50) and planar scintigraphy (51). These studies demonstrated high reproducibility for healthy subjects (49,51), chronic obstructive pulmonary disease (COPD) patients (48), and pediatric cystic fibrosis patients (50) at least over a time frame of 1 day in contrast to our findings. The reproducibility of 4D CT ventilation imaging would be deteriorated by variations arising from several factors. One of the important factors would be respiratory variation during 4D CT scans. Four-dimensional CT images are created by acquiring oversampled CT data segments at multiple couch positions over multiple respiratory cycles. Respiratory variations result in mismatches in the respiratory phase between CT data segments, which manifest as artifacts in 4D CT images at an alarmingly high frequency (52). Thus, we attempted to relate the temporal variation in ventilation to the temporal variation in abdominal motion range as a measure of the depth of breathing, which resulted in a moderate, significant relationship overall based on both the global and regional analyses. Our results indicate that the reproducibility of 4D CT ventilation imaging could be increased by decreasing respiratory variation during 4D CT scans. Abdominal motion range–based linear normalization did not improve the reproducibility of 4D CT ventilation imaging, which was at least in part due to uncertainties in the relationship between the motion range variation and ventilation variation as reflected by large error bars in Figures 5b and 6b. The large uncertainties would be because the motion ranges were calculated from the abdominal displacements that provide only global information for each CT data segment, whereas regional ventilation would likely change with breathing nonuniformly. In addition, there were deformed exhale voxels that belonged to two different CT data segments especially around the segment interface in ventilation computation. However, any such effect was not taken into account when calculating motion ranges, which would introduce uncertainties to the voxel-by-voxel correspondence between the motion range and ventilation. Several patients demonstrated nonsignificant relationships between the motion range variation and ventilation variation, which may be due to weak correlations between the abdominal motion and lung volume change. Iwasawa et al reported emphysematous patients showing paradoxical motion of the diaphragm (53,54). Also there have been several studies demonstrating varying correlations between the external respiratory signal and internal motion (eg, diaphragm and lung tumor) (55–57). Considering these studies, we cannot rule out possibility of weak correlations between the abdominal motion and lung volume change for our patient cohort. Spirometry provides lung volume information, and hence may improve the relationship with the ventilation variation.

For the different-day cohort, the reproducibility of 4D CT ventilation imaging could be deteriorated by additional variations arising from image acquisition, image registration, and

underlying physiologic change. Although the same 4D CT scan parameters were used in the two repeat scans, there were several considerable differences including patient's arm position (up or down) and the use of the immobilization devices. Couser et al investigated the respiratory consequences of arm elevation during tidal breathing and demonstrated significant increases in ventilatory and metabolic requirements for simple arm elevation compared to arms down (58). The difference in arm position might also contribute to the temporal variation in regional ventilation. Variations in arm position and the use of immobilization devices would also lead to variation in patient's anatomy that impacts image registration between the two 4D CT images, even though the lung volumes in the two scans were comparable to each other for both the peak-exhale and peak-inhale phases. The air volumes in the lungs were markedly different between the two scans. The cause is not clear; however, it might be due to the uncertainty in estimating the air volume by Equation 4. Furthermore, underlying physiologic changes might occur because of tumor growth and/or airway narrowing or closure in COPD for example. Mathew et al found moderate reproducibility for the ventilation defect volume measured by repeat hyperpolarized ^{3}He MR imaging over a 7-day time frame, while they found high reproducibility over a 7-minute time frame for 24 subjects including healthy volunteers and COPD patients (48). They explained that lower reproducibility for the 7-day time frame might be due to physiologic changes in COPD. Nevertheless, these variations were considered to be minimal in this study, given that the reproducibility of 4D CT ventilation imaging for the different-day cohort was comparable to that for the same-session cohort.

The findings from this study suggest that the reproducibility of 4D CT ventilation imaging could be increased by decreasing respiratory variation during 4D CT scans. In the literature, there have been several strategies to reduce respiratory variation for improved 4D CT imaging, including respiratory training (59–61) and respiration-synchronized acquisition (62–64). Also a new generation of multidetector CT (65) enables most of the thorax to be scanned at a single couch position, and hence would minimize respiratory variation. With these strategies, the reproducibility of 4D CT ventilation imaging may be increased.

Conclusions

We investigated the reproducibility of 4D CT ventilation imaging over the two different time frames of 15 days and 5 minutes for 12 patients. Four-dimensional CT ventilation images were found to be only moderately reproducible over the both time frames based on the voxel- and segment-wise analyses. Respiratory variation during 4D CT scans was found to be a significant factor that deteriorates the reproducibility. Improvement of 4D CT imaging would be necessary to increase the reproducibility of 4D CT ventilation imaging.

Acknowledgments

The authors thank Philips Radiation Oncology Systems for loaning Pinnacle^{3} treatment planning systems.

This study was supported in part by NIH/NCI R01 93626, Stanford Bio-X Grant and National Lung Cancer Partnership Young Investigator Research Grant.

References

1. Ling CC, Humm J, Larson S, et al. Towards multidimensional radiotherapy (MD-CRT): biological imaging and biological conformality. Int J Radiat Oncol Biol Phys. 2000; 47:551–560. [PubMed: 10837935]
2. Brahme A. Biologically optimized 3-dimensional in vivo predictive assaybased radiation therapy using positron emission tomographycomputerized tomography imaging. Acta Oncol. 2003; 42:123–136. [PubMed: 12801131]
3. Bentzen SM. Theragnostic imaging for radiation oncology: dose-painting by numbers. Lancet Oncol. 2005; 6:112–117. [PubMed: 15683820]
4. Marks LB, Spencer DP, Bentel GC, et al. The utility of SPECT lung perfusion scans in minimizing and assessing the physiologic consequences of thoracic irradiation. Int J Radiat Oncol Biol Phys. 1993; 26:659–668. [PubMed: 8330998]
5. Ireland RH, Bragg CM, McJury M, et al. Feasibility of image registration and intensity-modulated radiotherapy planning with hyperpolarized helium-3 magnetic resonance imaging for non-small-cell lung cancer. Int J Radiat Oncol Biol Phys. 2007; 68:273–281. [PubMed: 17448880]
6. Yaremko BP, Guerrero TM, Noyola-Martinez J, et al. Reduction of normal lung irradiation in locally advanced non-small-cell lung cancer patients, using ventilation images for functional avoidance. Int J Radiat Oncol Biol Phys. 2007; 68:562–571. [PubMed: 17398028]
7. Chen K, Chen X. Positron emission tomography imaging ofcancer biology: current status and future prospects. Semin Oncol. 2011; 38:70–86. [PubMed: 21362517]
8. Boersma LJ, Damen EM, de Boer RW, et al. A new method to determine dose-effect relations for local lung-function changes using correlated SPECT and CT data. Radiother Oncol. 1993; 29:110–116. [PubMed: 8310136]
9. Usenius T, Usenius JP, Tenhunen M, et al. Radiation-induced changes in human brain metabolites as studied by 1H nuclear magnetic resonance spectroscopy in vivo. Int J Radiat Oncol Biol Phys. 1995; 33:719–724. [PubMed: 7558964]
10. Munden RF, Erasmus JJ, Smythe WR, et al. Radiation injury to the liver after intensity-modulated radiation therapy in patients with mesothelioma: an unusual CT appearance. AJR Am J Roentgenol. 2005; 184:1091–1095. [PubMed: 15788578]
11. Seppenwoolde Y, Muller SH, Theuws JC, et al. Radiation dose-effect relations and local recovery in perfusion for patients with non-small-cell lung cancer. Int J Radiat Oncol Biol Phys. 2000; 47:681–690. [PubMed: 10837952]
12. Seppenwoolde Y, Engelsman M, De Jaeger K, et al. Optimizing radiation treatment plans for lung cancer using lung perfusion information. Radiother Oncol. 2002; 63:165–177. [PubMed: 12063006]
13. Das SK, Miften MM, Zhou S, et al. Feasibility of optimizing the dose distribution in lung tumors using fluorine-18-fluorodeoxyglucose positron emission tomography and single photon emission computed tomography guided dose prescriptions. Med Phys. 2004; 31:1452–1461. [PubMed: 15259648]
14. Christian JA, Partridge M, Nioutsikou E, et al. The incorporation of SPECT functional lung imaging into inverse radiotherapy planning for non-small cell lung cancer. Radiother Oncol. 2005; 77:271–277. [PubMed: 16274762]
15. McGuire SM, Zhou S, Marks LB, et al. A methodology for using SPECT to reduce intensity-modulated radiation therapy (IMRT) dose to functioning lung. Int J Radiat Oncol Biol Phys. 2006; 66:1543–1552. [PubMed: 17126212]
16. Lavrenkov K, Christian JA, Partridge M, et al. A potential to reduce pulmonary toxicity: the use of perfusion SPECT with IMRT for functional lung avoidance in radiotherapy of non-small cell lung cancer. Radiother Oncol. 2007; 83:156–162. [PubMed: 17493699]
17. Shioyama Y, Jang SY, Liu HH, et al. Preserving functional lung using perfusion imaging and intensity-modulated radiation therapy for advancedstage non-small cell lung cancer. Int J Radiat Oncol Biol Phys. 2007; 68:1349–1358. [PubMed: 17446001]

18. Gayed IW, Chang J, Kim EE, et al. Lung perfusion imaging can risk stratify lung cancer patients for the development of pulmonary complications after chemoradiation. J Thorac Oncol. 2008; 3:858–864. [PubMed: 18670303]
19. Zhang J, Ma J, Zhou S, et al. Radiation-induced reductions in regional lung perfusion: 0.1–12 year data from a prospective clinical study. Int J Radiat Oncol Biol Phys. 2010; 76:425–432. [PubMed: 19632063]
20. Ward ER, Hedlund LW, Kurylo WC, et al. Proton and hyperpolarized helium magnetic resonance imaging of radiation-induced lung injury in rats. Int J Radiat Oncol Biol Phys. 2004; 58:1562–1569. [PubMed: 15050337]
21. Cai J, Mata JF, Orton MD, et al. A rabbit irradiation platform for outcome assessment of lung stereotactic radiosurgery. Int J Radiat Oncol Biol Phys. 2009; 73:1588–1595. [PubMed: 19306756]
22. Ireland RH, Din OS, Swinscoe JA, et al. Detection ofradiation-inducedlung injury in non-small cell lung cancer patients using hyperpolarized helium-3 magnetic resonance imaging. Radiother Oncol. 2010; 97:244–248. [PubMed: 20724011]
23. Allen AM, Albert M, Caglar HB, et al. Can hyperpolarized helium MRI add to radiation planning and follow-up in lung cancer? J Appl Clin Med Phys. 2011; 12:3357. [PubMed: 21587180]
24. Guerrero T, Sanders K, Noyola-Martinez J, et al. Quantification of regional ventilation from treatment planning CT. Int J Radiat Oncol Biol Phys. 2005; 62:630–634. [PubMed: 15936537]
25. Simpson DR, Lawson JD, Nath SK, et al. Utilization of advanced imaging technologies for target delineation in radiation oncology. J Am Coll Radiol. 2009; 6:876–883. [PubMed: 19945044]
26. Yamamoto T, Kabus S, von Berg J, et al. Impact of four-dimensional computed tomography pulmonary ventilation imaging-based functional avoidance for lung cancer radiotherapy. Int J Radiat Oncol Biol Phys. 2011; 79:279–288. [PubMed: 20646852]
27. Ding K, Bayouth JE, Buatti JM, et al. 4DCT-based measurement of changes in pulmonary function following a course of radiation therapy. Med Phys. 2010; 37:1261–1272. [PubMed: 20384264]
28. Vinogradskiy YY, Castillo R, Castillo E, et al. Use of weekly 4DCT-based ventilation maps to quantify changes in lung function for patients undergoing radiation therapy. Med Phys. 2012; 39:289–298. [PubMed: 22225299]
29. Yamamoto T, Kabus S, Klinder T, et al. Four-dimensional computed tomography pulmonary ventilation images vary with deformable image registration algorithms and metrics. Med Phys. 2011; 38:1348–1358. [PubMed: 21520845]
30. Fuld MK, Easley RB, Saba OI, et al. CT-measured regional specific volume change reflects regional ventilation in supine sheep. J Appl Physiol. 2008; 104:1177–1184. [PubMed: 18258804]
31. Reinhardt JM, Ding K, Cao K, et al. Registration-based estimates of local lung tissue expansion compared to xenon CT measures of specific ventilation. Med Image Anal. 2008; 12:752–763. [PubMed: 18501665]
32. Ding, K., Cao, K., Amelon, RE., et al. Comparison of intensity- and Jacobianbased estimates of lung regional ventilation. Proc of the Third International Workshop on Pulmonary Image Analysis, MICCAI; 2010; p. 49-60.
33. Castillo R, Castillo E, Martinez J, et al. Ventilation from four-dimensional computed tomography: density versus Jacobian methods. Phys Med Biol. 2010; 55:4661–4685. [PubMed: 20671351]
34. Yamamoto, T., Kabus, S., von Berg, J., et al. Evaluation of four-dimensional (4D) computed tomography (CT) pulmonary ventilation imaging by comparison with single photon emission computed tomography (SPECT) scans for a lung cancer patient. Proc of the Third International Workshop on Pulmonary Image Analysis, MICCAI; 2010; p. 117-128.
35. Yamamoto T, Kabus S, Klinder T, et al. Investigation of four-dimensional computed tomography-based pulmonary ventilation imaging in patients with emphysematous lung regions. Phys Med Biol. 2011; 56:2279–2298. [PubMed: 21411868]
36. Castillo R, Castillo E, McCurdy M, et al. Spatial correspondence of 4D CT ventilation and SPECT pulmonary perfusion defects in patients with malignant airway stenosis. Phys Med Biol. 2012; 57:1855–1871. [PubMed: 22411124]
37. Du K, Bayouth JE, Cao K, et al. Reproducibility of registration-based measures of lung tissue expansion. Med Phys. 2012; 39:1595–1608. [PubMed: 22380392]

38. Rietzel E, Pan T, Chen GT. Four-dimensional computed tomography: image formation and clinical protocol. Med Phys. 2005; 32:874–889. [PubMed: 15895570]
39. Kabus S, Lorenz C. Fast elastic image registration. Proc Med Image Analysis Clinic - A Grand Challenge, MICCAI. 2010:81–89.
40. Kabus, S., Klinder, T., Murphy, K., et al. Evaluation of 4D-CT Lung Registration. In: Yang, GZ.Hawkes, DJ.Rueckert, D., et al., editors. Proc MICCAI. London, UK: 2009. p. 747-754.
41. Kabus, S., von Berg, J., Yamamoto, T., et al. Lung ventilation estimation based on 4D-CT imaging. Proc First International Workshop on Pulmonary Image Analysis, MICCAI; 2008; p. 73-81.
42. Guerrero T, Sanders K, Castillo E, et al. Dynamic ventilation imaging from four-dimensional computed tomography. Phys Med Biol. 2006; 51:777–791. [PubMed: 16467578]
43. Hoffman EA, Ritman EL. Effect of body orientation on regional lung expansion in dog and sloth. J Appl Physiol. 1985; 59:481–491. [PubMed: 4030600]
44. Dice LR. Measures of the amount of ecologic association between species. Ecology. 1945; 26:297–302.
45. Zou KH, Tuncali K, Silverman SG. Correlation and simple linear regression. Radiology. 2003; 227:617–622. [PubMed: 12773666]
46. Landis JR, Koch GG. The measurementof observer agreement for categorical data. Biometrics. 1977; 33:159–174. [PubMed: 843571]
47. Zou KH, Warfield SK, Bharatha A, et al. Statistical validation of image segmentation quality based on a spatial overlap index. Acad Radiol. 2004; 11:178–189. [PubMed: 14974593]
48. Mathew L, Evans A, Ouriadov A, et al. Hyperpolarized 3He magnetic resonance imaging of chronic obstructive pulmonary disease: reproducibility at 3.0 tesla. Acad Radiol. 2008; 15:1298–1311. [PubMed: 18790402]
49. Parraga G, Mathew L, Etemad-Rezai R, et al. Hyperpolarized 3He magnetic resonance imaging of ventilation defects in healthy elderly volunteers: initial findings at 3.0 Tesla. Acad Radiol. 2008; 15:776–785. [PubMed: 18486013]
50. Woodhouse N, Wild JM, van Beek EJ, et al. Assessment of hyperpolarized 3He lung MRI for regional evaluation of interventional therapy: a pilot study in pediatric cystic fibrosis. J Magn Reson Imaging. 2009; 30:981–988. [PubMed: 19856418]
51. Amis TC, Crawford AB, Davison A, et al. Distribution of inhaled 99mtechnetium labelled ultrafine carbon particle aerosol (Technegas) in human lungs. Eur Respir J. 1990; 3:679–685. [PubMed: 2165917]
52. Yamamoto T, Langner U, Loo BW Jr, et al. Retrospective analysis of artifacts in four-dimensional CT images of 50 abdominal and thoracic radiotherapy patients. Int J Radiat Oncol Biol Phys. 2008; 72:1250–1258. [PubMed: 18823717]
53. Iwasawa T, Yoshiike Y, Saito K, et al. Paradoxical motion ofthe hemidiaphragm in patients with emphysema. J Thorac Imaging. 2000; 15:191–195. [PubMed: 10928612]
54. Iwasawa T, Kagei S, Gotoh T, et al. Magnetic resonance analysis of abnormal diaphragmatic motion in patients with emphysema. Eur Respir J. 2002; 19:225–231. [PubMed: 11866002]
55. Vedam SS, Kini VR, Keall PJ, et al. Quantifying the predictability of diaphragm motion during respiration with a noninvasive external marker. Med Phys. 2003; 30:505–513. [PubMed: 12722802]
56. Ahn S, Yi B, Suh Y, et al. A feasibility study on the prediction of tumour location in the lung from skin motion. Br J Radiol. 2004; 77:588–596. [PubMed: 15238406]
57. Hoisak JD, Sixel KE, Tirona R, et al. Correlation of lung tumor motion with external surrogate indicators of respiration. Int J Radiat Oncol Biol Phys. 2004; 60:1298–1306. [PubMed: 15519803]
58. Couser JI Jr, Martinez FJ, Celli BR. Respiratory response and ventilatory muscle recruitment during arm elevation in normal subjects. Chest. 1992; 101:336–340. [PubMed: 1735251]
59. Kini VR, Vedam SS, Keall PJ, et al. Patient training in respiratory-gated radiotherapy. Med Dosim. 2003; 28:7–11. [PubMed: 12747612]
60. George R, Chung TD, Vedam SS, et al. Audio-visual biofeedback for respiratory-gated radiotherapy: impact of audio instruction and audiovisual biofeedback on respiratory-gated radiotherapy. Int J Radiat Oncol Biol Phys. 2006; 65:924–933. [PubMed: 16751075]

61. Venkat RB, Sawant A, Suh Y, et al. Development and preliminary evaluation of a prototype audiovisual biofeedback device incorporating a patient-specific guiding waveform. Phys Med Biol. 2008; 53:N197–N208. [PubMed: 18475007]

62. Keall PJ, Vedam SS, George R, et al. Respiratory regularity gated 4D CT acquisition: concepts and proof of principle. Australas Phys Eng Sci Med. 2007; 30:211–220. [PubMed: 18044305]

63. Langner UW, Keall PJ. Prospective displacement and velocity-based cine 4D CT. Med Phys. 2008; 35:4501–4512. [PubMed: 18975697]

64. Langner UW, Keall PJ. Quantification of artifact reduction with real-time cine four-dimensional computed tomography acquisition methods. Int J Radiat Oncol Biol Phys. 2010; 76:1242–1250. [PubMed: 19939579]

65. Hein PA, Romano VC, Lembcke A, et al. Initial experience with a chest pain protocol using 320-slice volume MDCT. Eur Radiol. 2009; 19:1148–1155. [PubMed: 19137311]

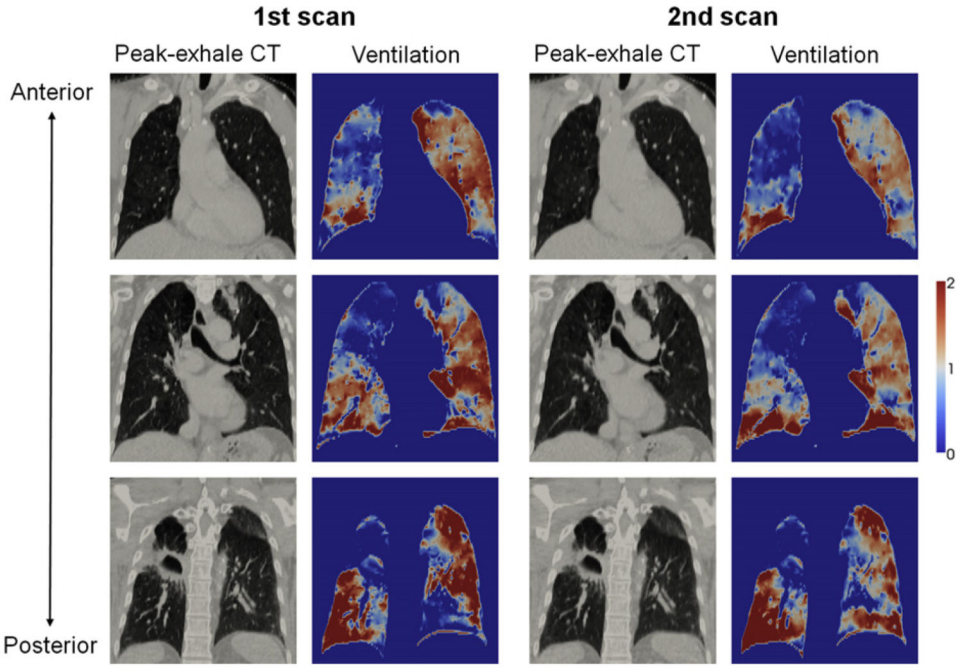

Figure 1.

Comparison of the first and second peak-exhale four-dimensional (4D) computed tomography (CT) and ventilation images at different coronal levels for patient 1 of the same-session cohort, showing the highest correlation in that cohort with the voxel-based Spearman correlation coefficient of 0.75. Note that ventilation is normalized by the overall mean value and that the second 4D CT and ventilation images are propagated to the domain of the first scan.

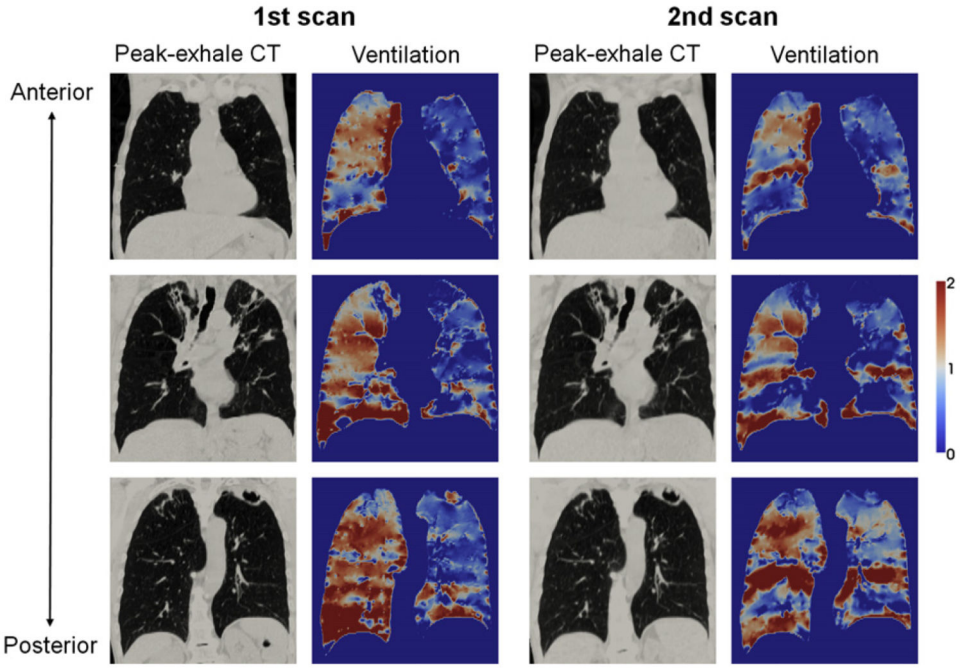

Figure 2.

Comparison of the 1st and 2nd peak-exhale four-dimensional (4D) computed tomography (CT) and ventilation images at different coronal levels for patient 6 of the different-day cohort, showing the lowest correlation in that cohort with the voxel-based Spearman correlation coefficient of 0.36. Note that ventilation is normalized by the overall mean value and that the second 4D CT and ventilation images are propagated to the domain of the first scan.

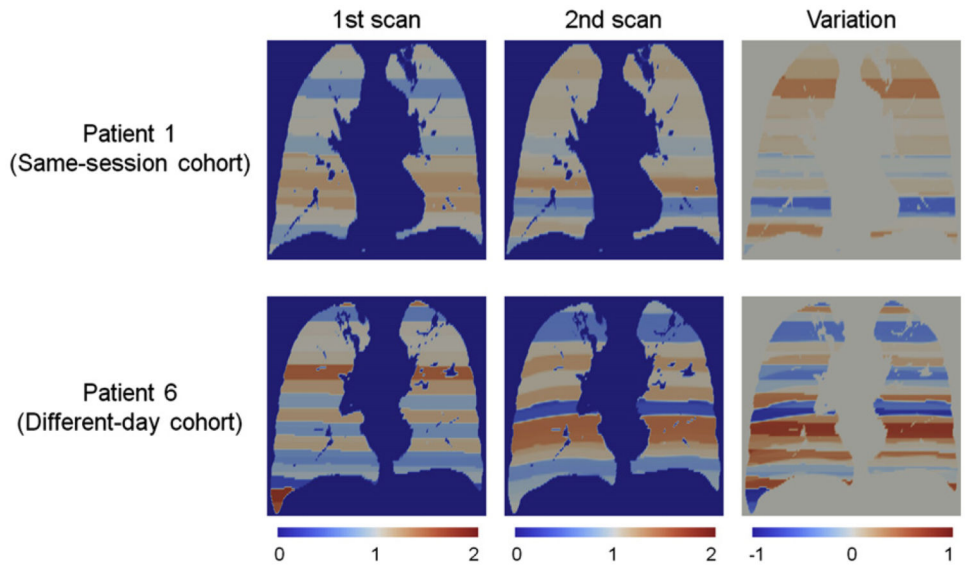

Figure 3.

Comparison of the abdominal motion range images of the first scan, second scan, and variation between the two scans for patient 1 of the same-session cohort and patient 6 of the different-day cohort. The standard deviation of motion range variation of patient 1 of the same-session cohort was 0.21, which was markedly smaller than 0.41 of patient 6 of the different-day cohort. Note that motion range is normalized by the overall mean value and that the second motion range images are propagated to the domain of the first scan.

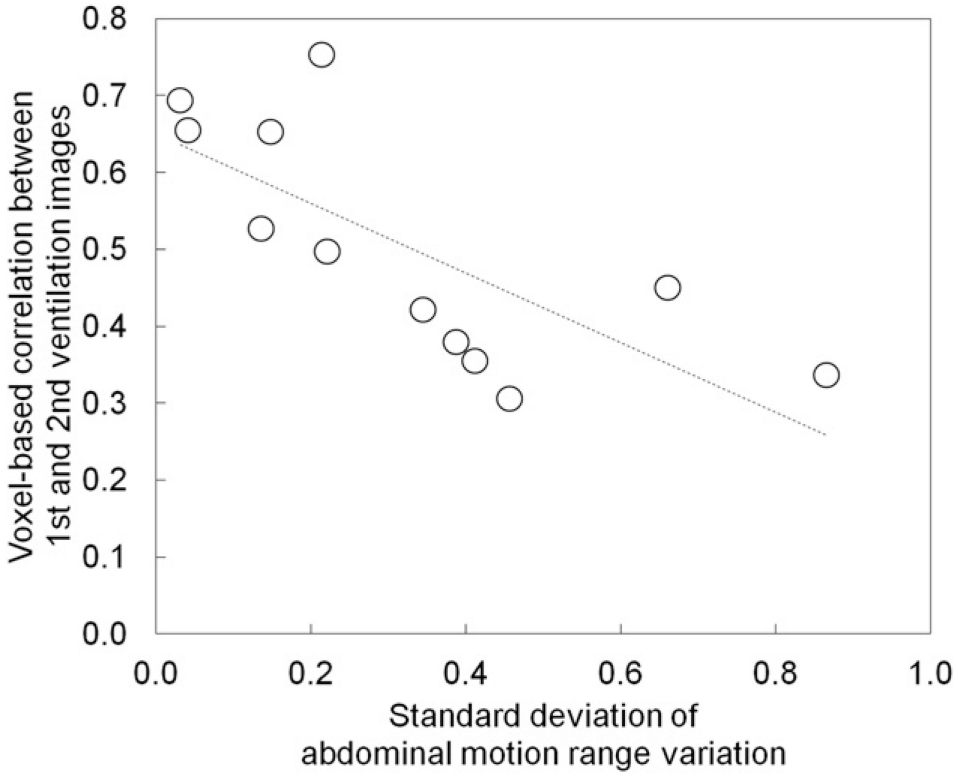

Figure 4.

Standard deviations of abdominal motion range variations versus voxel-based Spearman correlation coefficients between the first and second four-dimensional (4D) computed tomography (CT) ventilation images for 12 patients, showing a moderate, significant linear relationship ($r^2 = 0.55$, $P < .01$). The line of best fit is also shown.

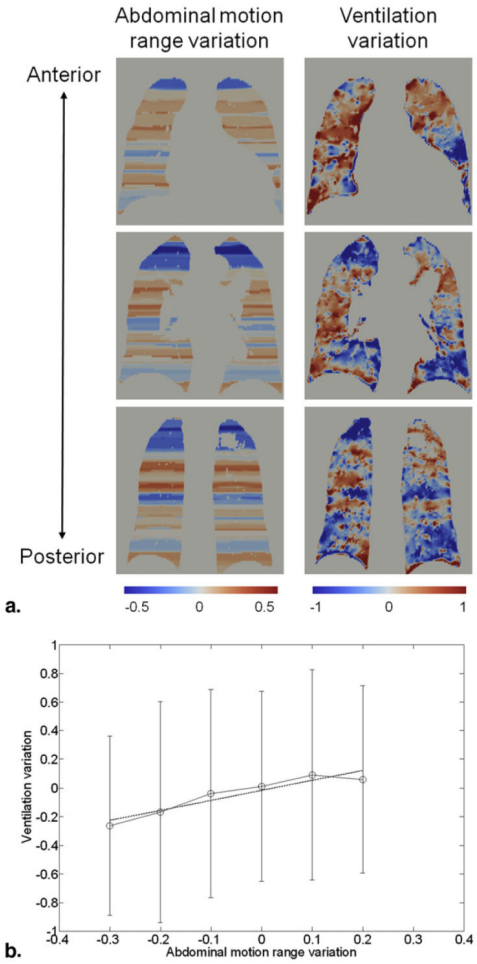

Figure 5.

(**a**) Comparison of the images of abdominal motion range variation and four-dimensional (4D) computed tomography (CT) ventilation variation at different coronal levels for patient 2 of the different-day cohort, showing the strongest linear relationship ($r^2 = 0.90$, $P < .01$). (**b**) Abdominal motion range variation versus 4D CT ventilation variation for the same patient. Points represent the average ventilation variations within motion range variation bins. Error bars represent the standard deviations.

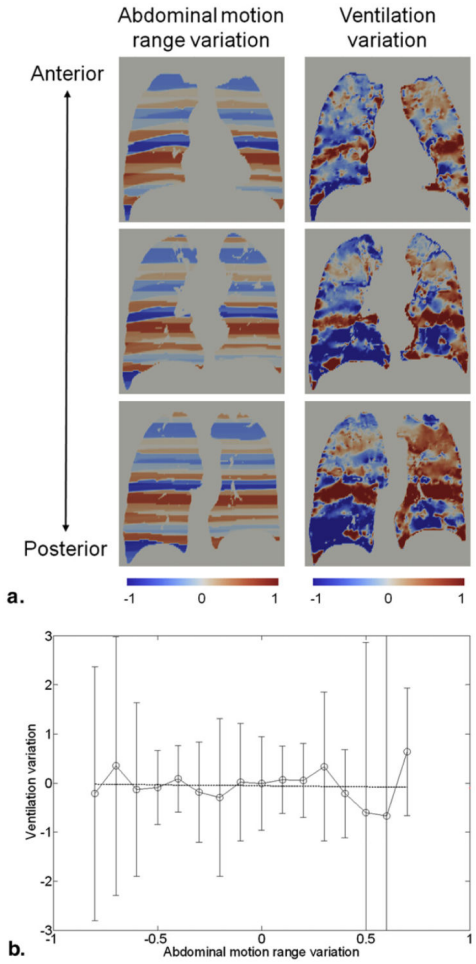

Figure 6.

(a) Comparison of the images of abdominal motion range variation and four-dimensional (4D) computed tomography (CT) ventilation variation at different coronal levels for patient 6 of the different-day cohort, showing the weakest linear relationship ($r^2 = 0.01$, $P = .83$). (**b**) Abdominal motion range variation versus 4D CT ventilation variation for the same patient. Points represent the average ventilation variations within motion range variation bins. Error bars represent the standard deviations.

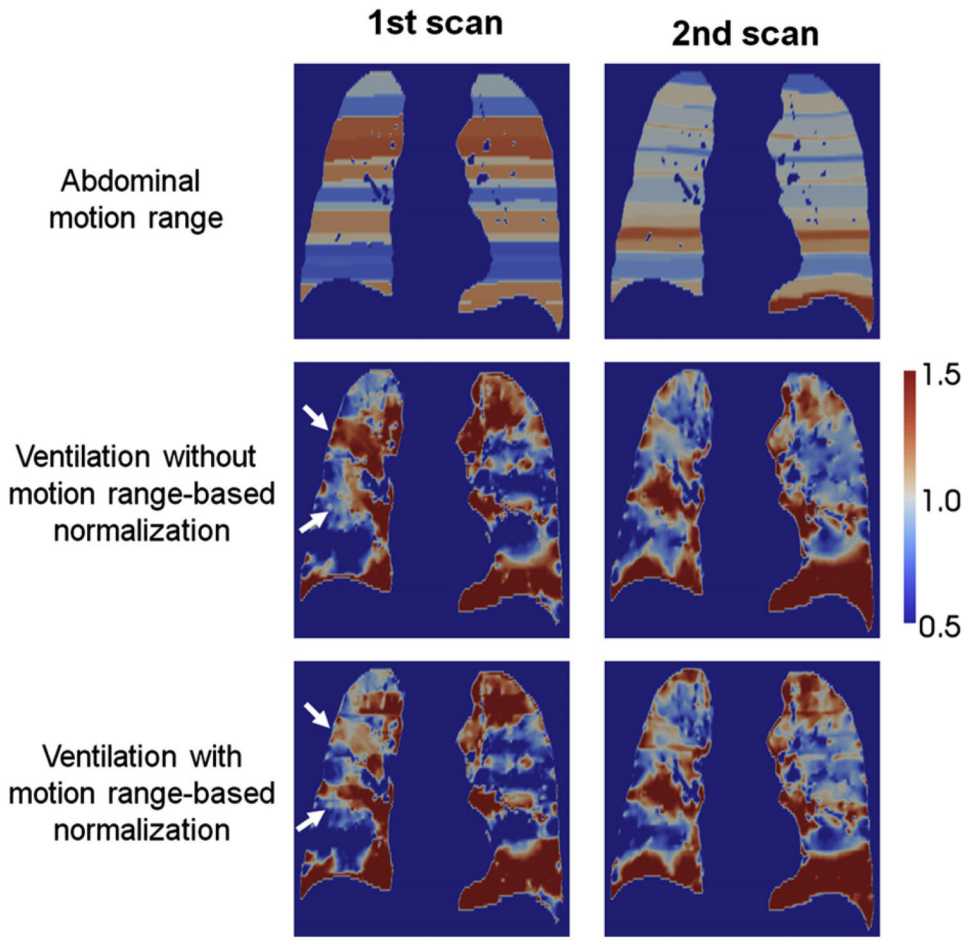

Figure 7.

Comparison of the images of the first and second abdominal motion range, and four-dimensional (4D) computed tomography (CT) ventilation without and with motion range-based linear normalization for patient 1 of the different-day cohort, showing the largest improvement in the voxel-based correlation between the two ventilation images from 0.50 to 0.56. Motion range-based normalization increased or decreased regional ventilation as denoted by white arrows in the first ventilation image and resulted in better agreements with the second ventilation image.

Table 1

Characteristics of Patients and Repeat 4D CT Scans for 12 Patients

Patient	Scan	Gender	Age (y)	Histology and Stage	Time Frame	AV Biofeedback Used?	Arm Position	ImmobilizationDevice Used?	Peak-exhale Lung (Air)Volume (cm^3)	Peak-inhale Lung (Air)Volume (cm^3)	Tidal Volume (cm^3)	Average Abdominal Motion Range (cm)
Different-day cohort												
1	First	Male	78	NSCLC, stage I	13 days	Yes	Up	Yes	4742 (3898)	5439 (4546)	648	1.25
	Second					Yes	Down	No	3863 (2912)	4936 (3706)	794	1.28
2	First	Male	66	NSCLC, stage III	12 days	Yes	Up	Yes	3681 (2889)	4055 (3241)	352	1.02
	Second					Yes	Down	No	3615 (1955)	4349 (2367)	412	1.37
3	First	Male	62	NSCLC, stage III	9 days	No	Up	Yes	5896 (4727)	6386 (5176)	449	0.64
	Second					No	Down	No	5537 (3897)	6532 (4481)	584	1.04
4	First	Male	82	NSCLC, stage IV	8 days	Yes	Up	Yes	7812 (6694)	8130 (6983)	289	0.43
	Second					Yes	Up	Yes	8436 (4993)	9021 (5492)	499	0.51
5	First	Male	67	NSCLC, stage IV	30 days	Yes	Up	Yes	5021 (4019)	5735 (4710)	691	0.97
	Second					Yes	Up	Yes	4748 (3307)	5655 (4108)	800	0.97
6	First	Male	77	NSCLC, stage II	15 days	No	Up	Yes	6622 (5663)	7126 (6142)	479	0.95
	Second					No	Down	No	6145 (4771)	6624 (5211)	441	0.95
Same-session Cohort												
1	First	Male	60	NSCLC, stage IV	5 min	No	Down	Yes	3470 (2579)	3712 (2869)	290	0.65
	Second					Yes	Down	Yes	3508 (2579)	3837 (2853)	275	0.64
2	First	Female	74	NSCLC, stage I	6 min	Yes	Down	Yes	2837 (1887)	3430 (2445)	558	0.66
	Second					No	Down	Yes	2645 (1765)	3356 (2369)	604	0.65
3	First	Male	61	NSCLC, stage I	5 min	No	Up	Yes	4382 (3448)	4711 (3719)	272	0.59
	Second					Yes	Up	Yes	4564 (3404)	4971 (3705)	301	0.57
4	First	Female	57	Metastatic tumor	5 min	Yes	Up	Yes	1418 (854)	2004 (1397)	543	0.95
	Second					No	Up	Yes	1375 (822)	1786 (1240)	418	0.62
5	First	Male	59	NSCLC, stage III	5 min	No	Up	Yes	4257 (3428)	4860 (3993)	566	0.74
	Second					Yes	Up	Yes	4839 (3343)	5020 (3859)	516	0.36
6	First	Female	67	NSCLC, stage III	4 min	No	Up	Yes	2467 (1884)	2879 (2266)	382	0.66
	Second					Yes	Up	Yes	2575 (1823)	2953 (2187)	364	0.70

4D, four-dimensional; AV, audiovisual; CT, computed tomography; NSCLC, non–small-cell lung cancer.

Table 2

Voxel-based Spearman Correlation Coefficients (All Voxels within the Lung) and Dice Similarity Coefficients (Segmented Functional Lung Volumes) between the First and Second Four-dimensional Computed Tomography Ventilation Images for 12 Patients

		Dice Similarity Coefficient		
Patient	**Voxel-based Correlation**	**High**	**Moderate**	**Low**
Different-day cohort				
1	0.50	0.57	0.43	0.56
2	0.65	0.66	0.44	0.65
3	0.38	0.56	0.40	0.47
4	0.45	0.56	0.46	0.56
5	0.53	0.60	0.44	0.54
6	0.36	0.54	0.44	0.53
Mean ± SD	0.48 ± 0.11	0.58 ± 0.0	5 0.44 ± 0.02	0.55 ± 0.06
Same-session cohort				
1	0.75	0.72	0.59	0.76
2	0.66	0.64	0.47	0.67
3	0.42	0.60	0.49	0.57
4	0.69	0.74	0.54	0.67
5	0.34	0.49	0.38	0.52
6	0.31	0.51	0.46	0.51
Mean ± SD	0.53 ± 0.20	0.62 ± 0.1	1 0.49 ± 0.07	0.62 ± 0.10
All patients				
Mean ± SD	0.50 ± 0.15	0.60 ± 0.0	8 0.46 ± 0.06	0.58 ± 0.09

Table 3

Slopes, r^2, and *P* Values of the Linear Regression Models for the Relationship between the Abdominal Motion Range Variation and Four-dimensional Computed Tomography Ventilation Variation for 12 Patients

Patient	Slope	r^2	*P* Value
Different-day cohort			
1	0.88	0.81	<.01
2	0.70	0.90	<.01
3	0.48	0.29	.06
4	0.30	0.23	.03
5	0.55	0.35	.30
6	−0.04	0.01	.83
Same-session cohort			
1	0.33	0.07	.44
2	1.11	0.85	<.01
3	0.17	0.02	.65
4	1.03	0.83	<.01
5	0.35	0.28	<.01
6	0.46	0.41	.01
All patients			
	0.26	0.42	<.01